Evaporation-based Microfluidic Pump Using Super-Hydrophilic Diatom Biosilica Thin Films

Hunter Jarrett[1], Micah Wade[1], Joseph Kraai[2], Gregory L. Rorrer[2], Alan X. Wang[3], Hua Tan[1]
1 School of Engineering and Computer Science,
Washington State University-Vancouver, Vancouver, WA, 98686, USA
2 School of Chemical, Biological and Environmental Engineering,
Oregon State University, Corvallis, OR, 97331, USA
3 School of Electrical Engineering and Computer Science,
Oregon State University, Corvallis, OR, 97331, USA

Abstract

Diatoms are a group of single-celled photosynthetic algae that use biochemical pathways to bio-mineralize and self-assemble three-dimensional photonic crystals with unique photonic and micro- & nano-fluidic properties. In recent years, diatom biosilica has been used in surface-enhanced Raman scattering (SERS) based optofluidic sensors for detection of a variety of chemical and biological molecules. In this paper, we present a study to develop a microfluidic pumping system using super-hydrophilic diatom thin films. The desire to develop such a system stems from the requirement to create a low-cost, self-powered microfluidic pumping system that can sustain a continuous flow over an extended period of time. The diatom biosilica acts not only as the driving force behind the flow, but also serves as ultra-sensitive SERS substrates that allows for trace detection of various molecules.

Liquid is drawn from a reservoir to the tip of a 150μm inner diameter capillary tube positioned directly over the diatom film. A thin and long horizontal reservoir is used to prevent flooding on the diatom film when the liquid is initially drawn to the diatom film through a capillary tube from the reservoir. The connection of the meniscus from the capillary to the film was maintained from a horizontal reservoir for a recorded time of 20 hours and 32 minutes before the partially filled reservoir emptied. Flow rates of 0.38, 0.22 and 0.16μL/min were achieved for square biosilica thin films of 49mm^2, 25mm^2, and 9mm^2 at a temperature of 63℉ and 45% relative humidity respectively. A temperature-controlled system was introduced for the 49mm^2 substrate and flow rates of 0.60, 0.82, 0.93, and 1.15μL/min were observed at 72, 77, 86, and 95℉ at 21% relative humidity respectively. More testing and analysis will be performed to test the operation limits of the proposed self-powered microfluidic system.

Keywords: Diatom, Surface Enhanced Raman Scattering (SERS), Biosilica, Microfluidic, Pump, Super-hydrophilic, Thin Films

Introduction

Microfluidic lab on chip (LOC) research has increased over the past decade because of its ability to reduce cost, sample size and process times[1]. Using key properties of fluid transport phenomena (e.g., surface tension, capillary action, and pressure), microfluidic technology has been employed in insulin delivery systems, micro heat exchangers, and chemical/biological optofluidic detection systems[1–3].

The ability to transport fluids precisely and continuously in microfluidic devices is critical for successful operation[4]. Several micro-pumping techniques have been developed and can be classified into two categories: a) active pumps, which require an external power source to pump the fluid and b) passive pumps, which use inherent fluid properties and geometric effects at the microscale to instigate flow[2]. Active micro-pumps employ either mechanical or non-mechanical techniques to drive flow. Active mechanical pumps generate flow through oscillation or rotation of a mechanical device, typically a piezo actuator, whereas active non-mechanical micro-pumps have utilized electro- and magneto-kinetic, acoustic, chemical, and bubble-driven pumping techniques[2]. Mechanical pumps provide the user with a large amount of control over flowrate but have faced

several limitations including complexity, high cost, complex structures, damage to living cells, and large fluid dead volumes[5–7]. Active non-mechanical pumps are capable of accurately transporting small amounts of fluid because they lack the necessity for large dead volumes to operate, but still rely on external signals to initiate and cease pumping, increasing their cost and complexity, making them undesirable for point-of-care diagnostic applications. Passive pumping is desirable because it uses intrinsic properties of the fluid, such as capillary action, and geometric relations to induce flow. Passive pumping is desirable because it is simple, allows for chip size reduction, and makes devices more portable. The primary limitation with capillary flow is that once an entire capillary surface is wetted, the energy driving the flow ceases.

Inspired by the fluidic transportation network in plants, several researchers have investigated coupling evaporation with capillary action to pump fluid in mico and nano scale devices[4,6–21]. Surface area, temperature, humidity and the velocity of air passing over the surface of a liquid impact the rate of evaporation, which equals to the flowrate in the device at steady state [7,9,11,13,17,18,20]. Active capillary-

evaporation (CE) pumps use temperature control or forced air to increase and/or control flowrate in microfluidic devices, whereas passive CE pumps operate under room temperature and relatively stagnant air conditions, meaning that flowrate is determined by the environment. Active CE pumps are relatively simple and can achieve precise flowrate control by using feedback loops coupled with algorithms to control temperature and air speed. However, electronics aren't always practical, complicate the system, and increase a device's size. Passive CE pumps require no external power, leading to low cost, efficient, and transportable microfluidic devices. Another factor that affect efficiency of CE pumps is the medium that they are evaporating from. Open channels, gels, and porous media have been used to control CE flowrates in the past. Table 1 provides a list of previous active/passive CE pump experiments, flowrates, evaporation mediums, and the duration that pumping action was maintained.

Table 1: Previous Evaporation Pumping Studies (U=Unknown, Operating Times are Approximate)

Reference/ Date of Study	Active Method	Flowrate (µL/hr)	Evaporation Medium	Operating Time
Junker/ 2002[20]	Airflow	72	Open Channel	U
Juncker/ 2002[20]	-	2.9	Open Channel	U
Effenhauser/ 2002[12]	-	0.6-60	Adsorption Agent	Days
Goedecke/ 2002[6]	Airflow	25	Open Channel	U
Namasivayam/ 2003[11]	Airflow/Heat	0.3	Open Channel	2 hrs
Zimmerman/ 2005[10]	Heating/Temperature Modulation	4.3	Open Channel	U
Guan/ 2006[8]	-	181	Open Channel	U (Several Hours)
Xu/ 2008[17]	-	32.4-140	Rolled Filter Paper	400 hrs
Choi/ 2009[19]	-	0.008-0.032	Porous Dehydrating Gel Exposed to Air	6 hrs
Chen/ 2012[7]	-	31.8	Porous Filter	U
Chen/ 2012[17]	Heater	800	Porous Filter	U
Zhang/ 2014[21]	Piezoelectric	84.6	Water Absorbing Paper	U
Nie/ 2015[18]	-	0.44-7.2	Porous Structure	U
Kim/ 2016[13]	Heaters	30	Micro Porous Hydrogel	Days

We propose using diatom biosilica based porous structures to drive continuous flow in microfluidic devices over long period of time because of their super hydrophilic properties. Diatoms are a group of single-celled photosynthetic algae made of silica [22,23] that use biochemical pathways to bio-mineralize and self-assemble unique, highly ordered and hierarchical three-dimensional photonic crystal biosilica with nanoporous structures [23,24]. Interest in integrating diatoms into micro- and nano-scale devices has grown over the past several years because of their photonic crystal properties, photoluminescence effects, and intricate, patterned shells called frustules [23,25–27]. Researchers are currently looking at integrating diatoms into systems pertaining to chemical/biological

detection, solar batteries, electroluminescent devices, drug delivery, microfluidic transport, and grown 3D nano-computers [24,27]. Several studies have already confirmed that diatoms are feasible for chemical and biological detection in optofluidic devices using surface-enhanced Raman scattering (SERS) and fluorescence after they undergo specific processes that either genetically engineer them or that synthesize the diatom frustules with nanoparticles[23,26,27]. For example, by using a photonic crystal biosilica SERS substrate by the synthesized diatom frustules with silver nanoparticles, we were able to detect trinitrotoluene (TNT) down to 10^{-10} M in concentration[23]. Such detection capability coupled with the super hydrophilic diatom porous structure

means that diatoms can simultaneously serve dual purposes: passive pumping (porous evaporator) and optical sensing. By combining pumping and sensing into one component, the size, complexity and cost of the microfluidic sensor can be significantly reduced.

This study creates an evaporation-based pump that uses a thin porous film of Pinnularia sp. Biosilica as a driving capillary force to pump liquid from a reservoir into the film. Once the biosilica is completely wetted evaporation will cause a continuous flow from the reservoir to the substrate. Proof of concept and approximate flow rates are determined visually and by using image processing tools in MATLAB. This paper provides and overview of experimental methods, initial analysis, and future work. The desire to develop such a pumping system stems from its applicability in optofluidic biosensors capable of ultra-sensitive detection of chemical and biological molecules using surface-enhanced Raman scattering. This study is the first to use evaporating menisci in porous media with nanoscale pores to drive fluid flow in microfluidic systems. Experiments are carried out on square films ranging from 9 mm^2 to 49 mm^2 with varying types of reservoirs and atmospheric conditions. By combining the pump and analysis portion of a microfluidic system into a single component, a smaller, cheaper, and more efficient microfluidic device capable of accurately detecting nano molecules in picolitre solutions will be realized.

Experimental Methods

Materials

The multi-layered Pinnularia sp. diatom biosilica frustule films used in the experiment were grown using a drop cast film fabrication method on microscope slides. Slides were prepared by cleaning them in solution with an ultrasonic bath, rinsing them, and treating them with a UV-Ozone cleaner. Once the slides were prepared, biosilica were suspended in a water or ethanol solution and deposited with a pipette onto preheated slides in a petri dish. Over time, the liquid evaporates, leaving a thin bioslica film on the substrate. The films are then heat treated to oxidize residual organic contaminants and to fix the biosilica to the substrate's surface. Square films of 9, 25, and 49 mm^2 with thicknesses of approximately 25μm were fabricated as shown in Fig. 1 and used to collect data. In all experiments, deionized water is used.

Microfluidic assembly

The microfluidic device consists of a reservoir made of 1mL pipette, a capillary tube, and the diatom chip as shown in Fig 2. The reservoir is a Fisherbrand™ Kolmer Serological Pipette with a 2.71mm inner diameter as shown in Fig 3. The capillary tube of a 150μm inner diameter, purchased from Lab Smith, is

made of polyetheretherketone (PEEK). The adhesive used to join the two together is Clear Silicone Waterproof Sealant by Loctite. The orifice of the capillary tube is made in contact with the edge of the diatom chip to enable the flow from the pipette to the hydrophilic diatom chip during the experiment.
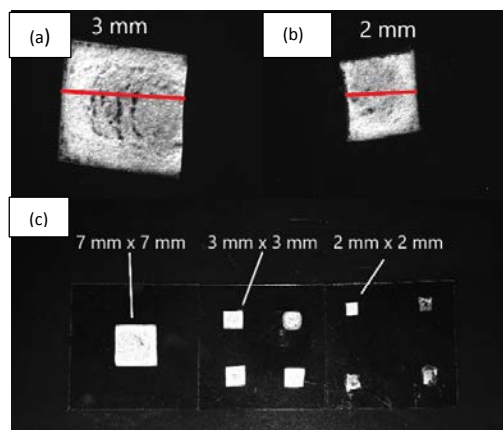
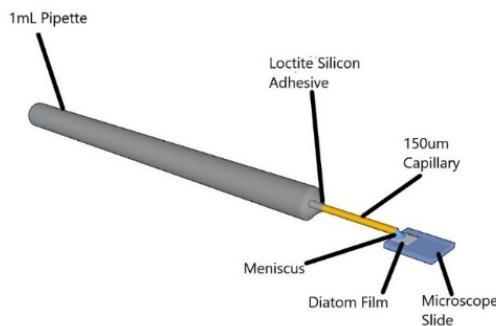Figures 1: (a) 3mm Diatom Film (b) 2mm Diatom Film, and (c) 7mm, 3mm and 2mm Diatom Films

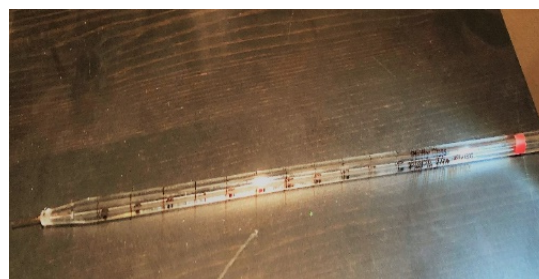Figure 2: Diagram of Pumping System

Figure 3: Actual Image of Pipette and Capillary

Visualization setup

In order to study the evaporation driven capillary flow, we designed an apparatus to hold the microfluidic assembly in place and visualize the flow. Our visualization setup consists of a custom base, camera clamp, light holder, slide stage, x, y, and z linear slide rails, and a pipette holder as shown in Fig. 4. A Thorlabs microscope slide clip is integrated into the apparatus to secure the diatom slides to the slide

stage. Our apparatus allows us to easily place the small orifice of the capillary tube in good contact with the top surface of the diatom chip and measure the flow rate during the experiment.

Images of the pipette, meniscus, and substrate were taken with a Phantom high-speed camera and a Thorlabs 1545M scientific camera using 12x and 6.5x Navitar microscope lenses respectively. The Phantom Camera used Vision Research software to record images and the ThorLabs camera used ThorCam software to record images. Temperature and humidity were initially measured using a Hygrometer Thermometer Clock with accuracies of +/- 1 °C and +/- 5% humidity respectively. Experiments involving a heating element used a DHT 22 temperature and humidity sensor to determine ambient temperature and humidity with a +/- 0.5 °C and 2-5% accuracy rating. An OMEGA(SRMU100101) heating element was used in conjunction with an Arduino Mega 2560, Adafruit 10K Precision Epoxy Thermistor-3950, and a solid-state relay to control the substrate temperature to within 1°C.
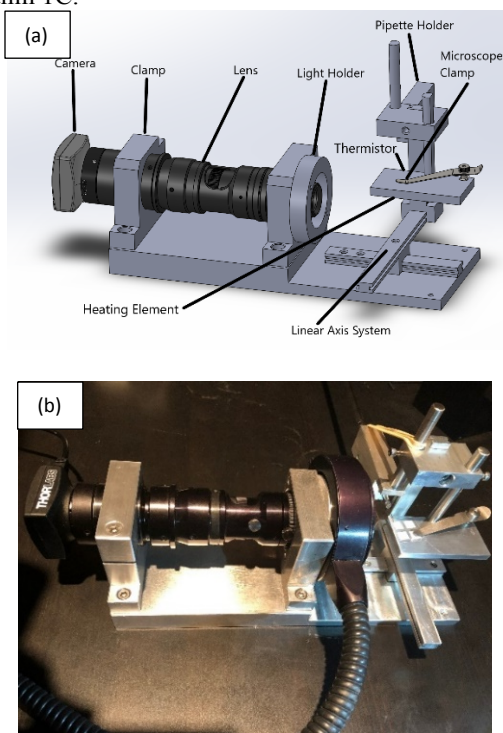

Figure 4: Apparatus and Imaging System: (a) schematics and (b) actual setup.

Results and Discussion

In our experiments, the pipette was initially filled with deionized (DI) water and placed in a horizontal position so that its body remained parallel to the ground. The pipette's vertical position was then adjusted until the tip of the capillary contacted the edge of the diatom film.

Flow was initiated using two different methods. In the first method, a pressure is applied at the end of the pipette, causing liquid to bulge and contact the film as shown in Figure 5 In the second method, a micro-droplet is dispensed onto the diatom film by a syringe, connecting the end of the capillary tube to the film. Both methods produced similar results and were implemented depending on the iteration of the set up.

When the liquid bulged from the pipette and contacted the diatom or was dropped onto the diatom surface, it initially formed a droplet (convex meniscus) on the diatoms surface shown in Figure 5 (a). Then, if the volume of the liquid was less than the volume of the diatom film, the liquid would be absorbed by the film, leading to the concave meniscus shown in Figure 5 (b). If the volume was greater than the volume of the diatom film, the liquid would absorb into the film and the positive pressure caused by the excess liquid in the convex meniscus would cause backflow into the capillary until the negative pressure caused by the diatom film balanced the capillary forces in the pipette, creating the same concave profile as shown in Figure 5 (b). Steady state was determined by timing how long a film took to go from a completely wetted appearance to a dry appearance and by monitoring the meniscus once the liquid contacted the film. The $49mm^2$ film took approximately 2 minutes to dry and the meniscus appeared to stabilize at approximately one minute. Initially, the consistency was being determined visually so, to ensure steady state, the systems was given 10 minutes to stabilize before any flowrate data was obtained. Later studies used a MATLAB imaging process to check meniscus stability to demonstrate steady-state. For the MATLAB imaging process, several images of the meniscus were taken over the course of 41 minutes. The meniscus was found and plotted, as shown in Figure 7. Because the meniscus position remained constant over time, it was determined that steady state was achieved.
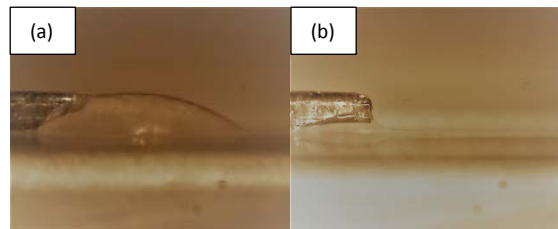

Figure 5: (a) Initial bulge outside the capillary tube from flow initiation and (b) steady meniscus outside the tube.

Evaporation driven continuous flow can be determined by observing the meniscus extending from the capillary tube using a microscope as well as macroscopically observing the diatom film. As shown in Figure 6, when the diatom film is wetted by the

water the diatom film remains translucent. During our experiments, we observed that the flow being pumped from the reservoir to the substrate by the strong negative pressure due to the micro-porous structure of the diatom film was recorded for a period of 20 hours and 32 minutes and the meniscus outside the capillary tube remains nearly constant throughout the experiment.
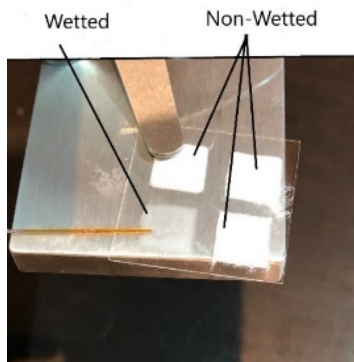
Figures 6: Visual comparison of wetted Film with dry film.
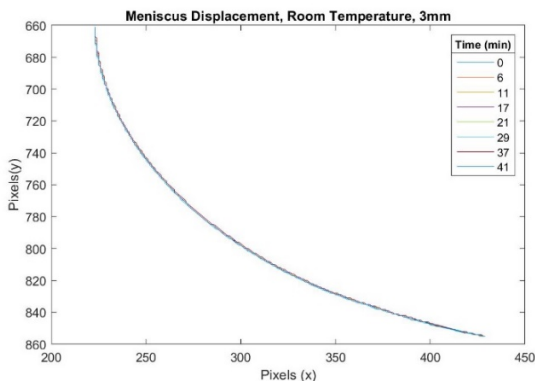

Figure 7: Meniscus Stability Over 41 Minutes

As the evaporation occurs in the diatom film, the meniscus in the pipette reservoir is receding according to mass conservation. In order to avoid the vacuum pressure formed in the empty region of the pipette due to receding of the meniscus in the pipette, we keep the end of the pipette open. Our experiments indicate that the evaporation from the open end of the pipette is negligible compared to that of the diatom film. Therefore, flowrate in our microfluidic system can be quantified by capturing the positions of meniscus inside the reservoir. For the initial 9, 25 and 49mm^2 film readings at 63℉, flowrates were visually estimated by using the pixel location at a specific point on the meniscus and using that same point in subsequent photos to quantify displacement. Subsequent experiments used MATLAB to find the maximum vertical location of the meniscus and track that location in succeeding photographs. Then a line was constructed using those points to determine pixel

displacement over time. A typical evolution of the receding meniscus in the pipette at different times is shown in Figure 8(b)-(d). To estimate the real distance between two pixels in the captured images, a high-precision calibration target of micrometer-scale marks is first taken in each experiment as shown in Figure 8 (a).
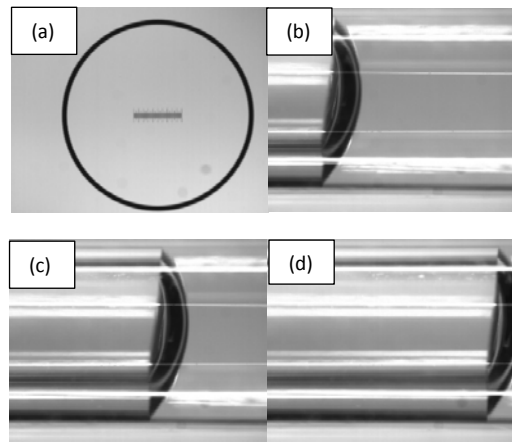
Figures 8: Process of 7mm×7mm film (a) calibrating scale for calculation pixel distance, (b) Initial Meniscus (0 minutes), (c) Intermediate Meniscus (27 minutes) and (d) Final Meniscus (53 minutes)

For the 49mm^2 and 9mm^2 films at 63℉, the time histories of the displacement of meniscus in the pipette reservoir are plotted in Figure 9. The meniscus displacement exhibited a linear trend over the analyzed portion of the pipette. A correlation between film surface area and flow rate was also noted for Figure 9. Increasing flowrates were observed at higher temperatures, as shown in Figure 10. At 72, 77, 86, and 95℉ and a relative humidity of approximately 21% for a 49mm^2 film, respective flow rates of 0.60, 0.82, 0.93, and 1.15μL/min were observed. The average total flow rate driven by the diatom film at 63 ℉ and 45% relative humidity of the 49mm^2, 25mm^2, and 9mm^2 was 0.38 μL/min, 0.22 μL/min and 0.16μL/min, respectively at 63 ℉ and 45% relative humidity, presented in Figure 11. The evaporation rate from the open end of a pipette not contacting the diatom film was determined to be approximately 0.004 μL/min and was neglected based on the order of magnitude. Flow was maintained for a maximum period of over twenty hours. The research so far has demonstrated system stability and that varied flowrates are achieved by modifying the area of the diatom film or by adjusting the temperature of the substrate. More accurate results and understanding of the system will come from analyzing different portions of the pipette, testing more film sizes to identify the trends between flow rate and surface area, and by comparing the results obtained in the lab to analytical solutions.
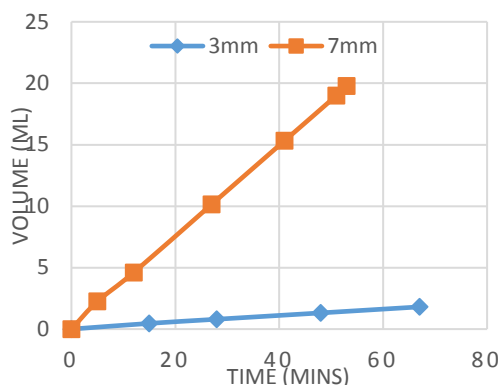
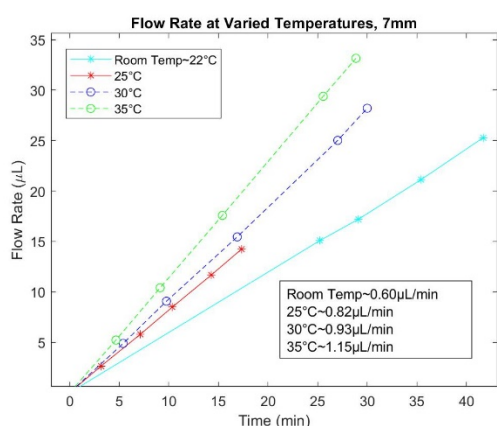Figure 9: Total flow in pipette reservoir over time

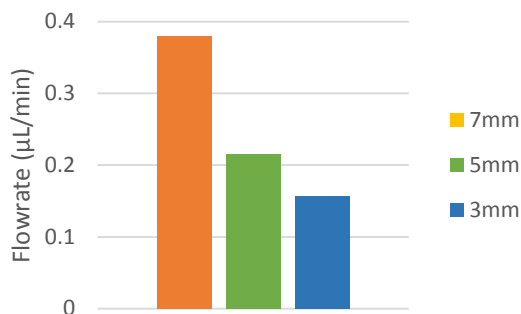Figure 10: Flow Rate for 7mm Substrate at Varied Temperatures

Figure 11: Averaged flowrates for 49mm^2, 25mm^2, and 9mm^2 films

Though flowrate in a small section of the reservoir exhibited linear trends, this relation should be tested at different portions of the reservoir. Hydraulic resistance is directly proportional to length[28] and as liquid is pumped from the reservoir, the resistance to flow should decrease. In addition to potential flow differences at varied positions of the reservoir, diatom films with different areas need to be observed using the new apparatus so that trends can be more clearly understood. Evaporation rate is proportional to area and should decrease with decreasing film area[29], as

demonstrated, but the full impact of area coupled with the porous structure needs to be studied in greater detail.

In our future work, the heating element will be used on different sized substrates so that surface area and temperature can be studied simultaneously to determine a maximum flow rate and to study flow rate patterns.

Conclusion

Flow from the study correlates nicely with previous passive evaporation-based flowrates, has been sustained for 20 hours and 32 minutes and displays linear flowrate patterns. Flowrates for 49, 25 and 9mm^2 films averaged 0.38, 0.22, and 016µL/min respectively, at 63̊F and 45% relative humidity. A 49mm^2 film highlighted the flow rates dependency on temperature by achieving 0.60, 0.82, 0.93, and 1.15µL/min flow rates at 72, 77, 86, and 95̊F respectively.

Displacements were obtained by using a microscopic scale of 1mm at a specific magnification. A picture was taken, and the lens positions were fixed. The picture of the scale was then analyzed to find a pixel distance for 1mm. Using this conversion, the pixel displacement in subsequent photos, and the known diameter of the pipette it was possible to determine flowrates.

Future work will focus on gathering more data concerning diatom film area and temperature in relation to evaporation rate. By using in-depth data analysis techniques in MATLAB's image processing software, precise and repeatable flowrate values will be obtained. Current data highlights trends over short displacements in the pipette and the flow rates dependency on film area and temperature.

REFERENCES
1. Ohno, K., Tachikawa, K. & Manz, A. Microfluidics: Applications for analytical purposes in chemistry and biochemistry. *Electrophor. Electrophor.* **29**, 4443–4453 (2008).
2. D J Laser. Areview of micropumps. *J. Micromechanics Microengineering* **14**, R35–R64 (2004).
3. IJMER Journal, R.M.Chanmanwar, R.Balasubramaniam & L.N.Wankhade. Application and Manufacturing of Microfluidic Devices: Review. (2014). doi:10.6084/M9.FIGSHARE.1041661.V1

4. Scott Lynn, N., Henry, C. S. & Dandy, D. S. Evaporation from microreservoirs. *Lab Chip Lab Chip* **9**, 1780 (2009).
5. WOIAS, P. Micropumpspast, progress and future prospects. *Sens. Actuators B Chem. Sens. Actuators B Chem.* **105**, 28–38 (2005).
6. Goedecke, N., Eijkel, J. & Manz, A. Evaporation driven pumping for chromatography application. *Lab Chip Lab Chip* **2**, 219 (2002).
7. Kuan-Yu Chen, Kuang-En Chen, Wang, K. & 2012 7th IEEE International Conference on Nano/Micro Engineered and Molecular Systems (NEMS). A flexible evaporation micropump with precision flow rate control for micro-fluidic systems. 653–656 (2012).
8. Guan, Y.-X., Xu, Z.-R., Dai, J. & Fang, Z.-L. The use of a micropump based on capillary and evaporation effects in a microfluidic flow injection chemiluminescence system. *Talanta* **68**, 1384–1389 (2006).
9. Zimmermann, M., Schmid, H., Hunziker, P. & Delamarche, E. Capillary pumps for autonomous capillary systems. *Lab. Chip* **7**, 119–125 (2006).
10. Zimmermann, M., Bentley, S., Schmid, H., Hunziker, P. & Delamarche, E. Continuous flow in open microfluidics using controlled evaporation. *Lab. Chip* **5**, 1355–1359 (2005).
11. Vijay Namasivayam. Transpiration-based micropump for delivering continuous ultra-low flow rates. *J. Micromechanics Microengineering* **13**, 261–271 (2003).
12. Effenhauser, C., Harttig, H. & Krämer, P. An Evaporation-Based Disposable Micropump Concept for Continuous Monitoring Applications. *Biomed. Microdevices* **4**, 27–32 (2002).
13. Hyejeong Kim, Kiwoong Kim & Sang Joon Lee. Compact and Thermosensitive Nature-inspired Micropump. *Sci. Rep.* **6**, (2016).
14. Antao, D. S. *et al.* Dynamic Evolution of the Evaporating LiquidVapor Interface in Micropillar Arrays. *Langmuir Langmuir* **32**, 519–526 (2016).
15. Du, X., Zhao, T. S. & Luo, J. Continuous micro liquid delivery by evaporation on a gradient-capillary microstructure surface. *J. Micromechanics Microengineering Struct. Devices Syst.* **21**, 095004 (2011).
16. Temiz, Y., Skorucak, J. & Delamarche, E. Capillary-driven microfluidic chips with evaporation-induced flow control and dielectrophoretic microbead trapping. **8976**, 89760Y-89760Y–10 (2014).
17. Xu, Z.-R. *et al.* A microfluidic flow injection system for DNA assay with fluids driven by an on-chip integrated pump based on capillary and evaporation effects. *Lab Chip Lab Chip* **8**, 1658 (2008).
18. Nie, C., Frijns, A. J. H., Mandamparambil, R. & Toonder, J. M. J. den. A microfluidic device based on an evaporation-driven micropump. (2015).
19. Choi, Y. H., Chung, K. H. & Lee, S. S. Microfluidic actuation by dehydration of hydrogel. *Sens. 2009 IEEE* 1370–1373 (2009). doi:10.1109/ICSENS.2009.5398421
20. Juncker, D. *et al.* Autonomous Microfluidic Capillary System. *Anal. Chem.* **74**, 6139–6144 (2002).
21. Zhang, A., Zha, Y. & Zhang, J. A surface acoustic wave micropump to pump fluids from a droplet into a closed microchannel using evaporation and capillary effects. *AIP Adv.* **4**, (2014).
22. Ever Aguirre, L. *et al.* Diatom frustules protect DNA from ultraviolet light. *Sci. Rep.* **8**, (2018).
23. Kong, X. *et al.* Detecting explosive molecules from nanoliter solution: A new paradigm of SERS sensing on hydrophilic photonic crystal biosilica. *Biosens. Bioelectron.* **88**, 63–70 (2017).
24. Jeffryes, C., Campbell, J., Li, H., Jiao, J. & Rorrer, G. The potential of diatom nanobiotechnology for applications in solar cells, batteries, and electroluminescent devices. *Energy Environ. Sci.* **4**, 3930–3941 (2011).
25. Kong, X. *et al.* Optofluidic sensing from inkjet-printed droplets: the enormous enhancement by evaporation-induced spontaneous flow on photonic crystal biosilica. *Nanoscale* **8**, 17285–17294 (2016).
26. Marshall, K. E., Robinson, E. W., Hengel, S. M., Pasa-Tolic, L. & Roesijadi, G. FRET Imaging of Diatoms Expressing a Biosilica-Localized Ribose Sensor. *PLoS One* **7**, (2012).
27. Gordon, R., Losic, D., Tiffany, M. A., Nagy, S. S. & Sterrenburg, F. A. S. The Glass Menagerie: diatoms for novel applications in nanotechnology. *TIBTEC Trends Biotechnol.* **27**, 116–127 (2009).
28. Kirby, B. *Physics of micro- and nano- scale fluid mechanics*. (Cambridge University Press, 2010).
29. Bergman, T. L., Lavine, A. S. & Incropera, F. P. *Fundamentals of Heat and Mass Transfer, 7th Edition*. (John Wiley & Sons, Incorporated, 2011).